Analyst

Portable Combination of Fourier Transform Infrared Spectroscopy and Differential Mobility Spectrometry for Advanced Vapor Phase Analysis

Journal:	*Analyst*
Manuscript ID	AN-ART-06-2018-001192.R1
Article Type:	Paper
Date Submitted by the Author:	17-Aug-2018

Complete List of Authors:	Hagemann, Tamina; Institut für Analytische und Bioanalytische Chemie, University of Ulm McCarteney, Mitchell; University of California, Davis, Department of Mechanical Engineering Fung, Alexander; University of California, Davis, Department of Mechanical Engineering Peirano, Daniel; University of California, Davis, Department of Mechanical Engineering Davis, Cristina; University of California, Davis, Department of Mechanical Engineering Mizaikoff, Boris; Institut für Analytische und Bioanalytische Chemie, University of Ulm

Journal Name

ARTICLE

Portable Combination of Fourier Transform Infrared Spectroscopy and Differential Mobility Spectrometry for Advanced Vapor Phase Analysis

Received 00th January 20xx,
Accepted 00th January 20xx

DOI: 10.1039/x0xx00000x

www.rsc.org/

L. Tamina Hagemann,[a,b] Mitchell M. McCartney,[a] Alexander G. Fung,[a] Daniel J. Peirano,[a] Cristina E. Davis,*[a] Boris Mizaikoff*[b]

Designing mobile devices for the analysis of complex sample mixtures containing a variety of analytes at different concentrations across a large dynamic range remains a challenging task in many analytical scenarios. To meet this challenge, a compact hybrid analytical platform has been developed combining Fourier transform infrared spectroscopy based on substrate-integrated hollow waveguides (iHWG-FTIR) with gas chromatography coupled differential mobility spectrometry (GC-DMS). Due to the complementarity of these techniques regarding analyte type and concentration, their combination provides a promising tool for the detection of complex samples containing a broad range of molecules at different concentrations. To date, the combination of infrared spectroscopy and ion mobility techniques remains expensive and bound to a laboratory utilitizing e.g. IMS as prefilter or IR as ionization source. In the present study, a cost-efficient and portable solution has been developed and characterized representing the first truly hyphenated IR-DMS system. As a model analyte mixture, 5 ppm isopropylmercaptan (IPM) in methane (CH_4) were diluted, and the concentration-dependent DMS signal of IPM along with the concentration-dependent IR signal of CH_4 were recorded for all three hybrid IR-DMS systems. While guiding the sample through the iHWG-FTIR or the GC-DMS first did not affect the obtained signals, optimizing the IR data acquisition parameters did benefit the analytical results.

Introduction

Infrared spectroscopy

In mid-infrared (MIR) absorption spectroscopy, molecular vibrations are excited via the absorption of photons in the 2-20 µm spectral regime.[1] Thus, obtained specific absorption patterns may serve as 'molecular fingerprints' for identifying and quantifying molecular analytes.[2] While a broad range of molecular species are readily identified via their vibrational fingerprint, complex real-world matrices demand complementary analytical techniques and advanced data evaluation routines for selective identification, classification, and quantification due to increasingly overlapping signals.

Substrate-integrated hollow waveguides pioneered by the Mizaikoff research team are photon conduits that simultaneously serve as miniaturized gas cells.[3–9] MIR radiation is guided via a hollow channel, which simultaneously accommodates minute volumes of gas or vapor phase samples. Given the compact dimensions of iHWGs, only few hundreds of microliters are probed, thereby ensuring particularly short transient times, and facilitating quasi-continuous measurements. Furthermore, iHWGs are robust and cost-efficient, and their shape, absorption path length, and surface coating may readily be tailored to specific application needs. Using iHWGs in combination with a variety of IR light sources ranging from FTIR spectrometers to quantum cascade and interband cascade lasers (QCLs, ICLs), detection limits (LOD) in the low percentage,[5] ppm[3,6,8] or the medium ppb[4,7] range were achieved.

Differential mobility spectrometry

Complementary analytical methods may provide significantly lower LODs such as differential mobility spectrometry (DMS). In DMS, the sample molecules are ionized and introduced into the space between two parallel planar electrodes by a carrier gas flow.[10,11] An asymmetric high-frequency voltage (i.e., RF voltage) is applied between the electrodes such that the time-averaged potential difference between the high and low field portion equals zero. Due to the movement induced by the carrier gas flow and the RF voltage, the ions are subject to a zig-zag trajectory in between the electrodes. They are either neutralized upon impact with one of the electrodes, or they reach the appropriate positive- or negative-ion detectors at the end of the drift tube, depending on their ion mobility at high and low electric fields. By additionally applying a

[a] Department of Mechanical and Aerospace Engineering, University of California Davis, CA 95616, USA. E-mail: cedavis@ucdavis.edu.
[b] Institute of Analytical and Bioanalytical Chemistry, Ulm University, 89081 Ulm, Germany. E-mail: boris.mizaikoff@uni-ulm.de.
†Electronic Supplementary Information (ESI) available: See DOI: 10.1039/x0xx00000x

compensation voltage (CV), part of the movement caused by the RF voltage may be compensated, thereby enabling different molecules (i.e., species with different ion mobilities) to reach the detector. In a chemical mixture, molecules compete for the ionization energy and their presence mutually influences their signal intensity. This issue can be accounted for in GC-DMS, where a GC column is coupled to the inlet of the DMS.[12] Here, the analytes are first temporally separated as they pass through the GC column, and then they are detected by the DMS. Furthermore, GC-DMS does not require continuous sample injection, and renders preconcentration feasible as chemicals are accumulated over time periods and released in discrete bursts into the system. When the RF voltage is constant, the obtained data is composed of the signal intensity (z) that depends on the CV (x) and the GC retention time (y). GC-DMS provides highly sensitive detection capabilities that is quantitative across the ppb and even ppt regime,[13,14] and a twofold separation[12] inherently based on two orthogonal principles, i.e., chromatographic separation and ion mobility. Therefore, GC-DMS[14–19] is highly suitable for studying complex mixtures at low concentrations, especially biological mixtures. Since the range of investigable analytes is limited by is ionization potential, a combination with complementary methods appears useful.

Combined infrared spectroscopy - ion mobility techniques

Since GC-DMS and iHWG-FTIR detect molecules in complementary concentration ranges based on orthogonal detection principles, the combination of these techniques provides a promising analytical system for the investigation of complex samples containing a variety of differently concentrated analytes such as those encountered in exhaled breath.

According to literature, IR techniques (e.g. FTIR,[20–24] DRIFT,[25] IRMPD[26–29]) and IM-based techniques (e.g. IMS,[30,31] DMS,[32] FAIMS[33,34]) have readily been applied to the same sample. The same sample was investigated separately by IR and IM providing orthogonal information, yet without hyphenating these methods onto one compact device. Alternatively, IR and an IM were combined utilizing e.g. the IR system as an ionization source serving the IM, and vice versa treating the IM as a prefilter for recording IR spectra of IM-selected molecules. Indeed, only Schindler *et al.*[34] have used spectral information from both IR and IM, yet in a laboratory-based setup.

Hence, to the best of our knowledge the present study represents the first integration of IR- and IM-based techniques into a single analytical setup in a cost-efficient and portable device format. The developed system enables complementary analysis of analytes at fundamentally different concentration levels across a wide dynamic range. Its utility for gas analysis was exemplarily demonstrated using mixtures of methane (CH_4) and isopropylmercaptan (IPM). IPM and CH_4 were specifically selected for demonstrating the orthogonality of the detection concepts, as their mixture could not have been detected with either of the techniques individually.

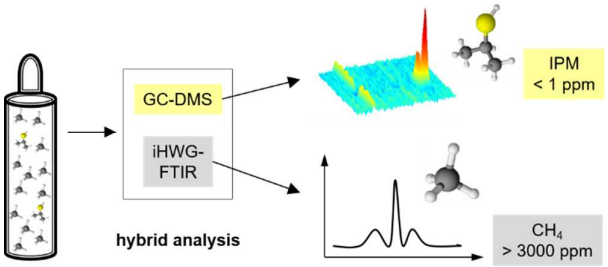

Fig. 1 A gaseous sample mixture of low concentrated isopropylmercaptan (ppb range) and highly concentrated methane (% range) was analyzed via the hybrid analytical setup interfacing GC-DMS and iHWG-FTIR taking advantage of the orthogonality of the two methods.

Experimental

Chemicals

IPM (5 ppm) dissolved in CH_4 was acquired from Matheson (Montgomeryville, PA, USA). The compressed air used to dilute the analyte mixture was taken from an in-house gas line and filtered with VOC filters (Restek, cat.# 21991). The gases were mixed via mass flow controllers (MFCs) from APEX (AX-MC-20SCCM-D/5M, AX-MC-100SCCM-D/5M, AX-MC500SCCM-D/5M).

iHWG-FTIR

The IR detection of methane was performed via a shoebox-sized ALPHA FTIR spectrometer (Bruker Optik GmbH, Ettlingen, Germany) using the software OPUS (version 7.2). Radiation emitted from the MIR source was coupled into an iHWG (see below for specifications) and onto a deuterated triglycine sulfate (DTGS) detector using gold-coated off-axis parabolic mirrors (Thorlabs, MPD254254-90-M01, 2” RFL) (see Figure S-1). An aluminum iHWG with an optical path length of 7.5 cm, a cross-section of 4x4 mm, and an inlet funnel structure was simultaneously serving as a light pipe and miniaturized gas cell. The channel was sealed via IR-transparent BaF_2 windows with a diameter of 6.65 mm and a thickness of 0.5 mm (OEC GmbH, Zusmarshausen, Germany). With the GC-DMS-IR(60) and the IR(60)-GC-DMS setup (see **Hybrid Setups**), the IR spectra were recorded in the spectral range of 4000 to 400 cm^{-1} at a spectral resolution of 8 cm^{-1}, with 10 scans averaged per measurement, and at a sample flow within the iHWG of 60 mL/min. With the IR(300)-GC-DMS setup, 2 cm^{-1} resolution, 20 averaged scans, and a flow rate of 300 mL/min were used. The Fourier transformation was executed using the Blackman-Harris 3-Term apodization function in OPUS. The IR setup was entirely housed in a plastic bag and permanently purged with VOC-filtered compressed air (Restek, cat.# 21991). PTFE tubing was used for all connections to avoid analyte adsorption.

GC-DMS

The GC-DMS analysis of IPM was performed using a suitcase-sized modified MicroAnalyzer (Sionex Corporation; see Figure S-2) using the software EXPERT (version 2.4.3). The

experimental procedure of the GC-DMS consisted of the following sequence: (i) preconcentration, (ii) separation via the GC column, and (iii) detection by the DMS. First, the sample was guided across a preconcentration trap filled with silica gel at 60 mL/min for 30 s. Traps were made of stainless steel tubes coated with SilcoNert® (SilcoTek, Bellefonte, Pennsyvlania, USA) to reduce sulfur reactions. In contrast to IPM, CH_4 was not preconcentrated by the silica gel trap. After the preconcentration, the trap was purged with room air for 5 s to avoid the accumulation of methane within the device. Directly after the preconcentration, the trap was heated from 50 °C to 115 °C, and kept at 115 °C for desorption and accumulation of analytes at the beginning of the GC column for 400 s. Subsequently, the trap was cooled to 50 °C. 125 s after the preconcentration phase, the GC column was heated from 50 °C to 150 °C at 50 °C/min, and kept at 150 °C for 650 s prior to cooling again to 50 °C. After progressing through the GC column at 1-5 mL/min, the analytes were led into the DMS for analytical identification. Ionization was performed via a ^{63}Ni source followed by detection by the DMS sensor (gap size 0.5 mm; RF waveform: 1250 V peak-to-peak-voltage, 1.2(±0.1) MHz, 30 % duty cycle; CV from -40 V to +15 V (200 steps and 2 s per full CV scan); flow 300 mL/min; sensor temperature 80 °C). In order to regenerate the silica gel prior to the next experiment, the trap was heated from 50 °C to 160 °C 520 s after the preconcentration phase ensuring complete desorption of the remaining molecules. The trap was then kept at 160 °C for 90 s before being cooled to 50 °C. The DMS settings were identical for all three hybrid setups.

Hyphenated IR-DMS systems

Three hybrid setups were realized, as displayed in Figure 2. In the GC-DMS-IR(60) setup (red), the sample was guided into the GC-DMS first (IPM detection) with the outlet of the preconcentration trap being connected to the iHWG (CH_4 detection). The FTIR settings for the GC-DMS-IR(60) setup were selected such that within the preconcentration phase of 30 s, the gas volume between the GC-DMS trap outlet and the iHWG was sufficiently purged with the analyte gas (i.e., gas volume exchanged twice) and such that the IR measurement was completed during the preconcentration phase for the GC-DMS.

In the IR(60)-GC-DMS and the IR(300)-GC-DMS setup (blue and blue/green, respectively), the sample was guided through the iHWG first, and then into the GC-DMS. In the GC-DMS-IR(60) and the IR(60)-GC-DMS setup, the flow in the iHWG and at the inlet of the GC-DMS was always 60 mL/min. In contrast, a split flow (4:1) was introduced between iHWG outlet and GC-DMS inlet in the IR(300)-GC-DMS setup, thereby enabling a higher flow rate of 300 mL/min into the iHWG while keeping the flow at the GC-DMS inlet at 60 mL/min, by diverting the excess gas flow of 240 mL/min. Also, different IR settings were used in the IR(300)-GC-DMS setup: in the GC-DMS-IR(60) setup, the IR analyte CH_4 leaves the GC-DMS at the GC-DMS sampling flow rate, and only during the DMS preconcentration phase. Therefore, the time available for IR measurements (i.e., also affecting the spectral resolution and number of averaged scans) and the flow in the iHWG are dictated by the preconcentration flow and the duration of the GC-DMS preconcentration phase. In the alternative configuration (iHWG first, then GC-DMS), the sample can flow through the iHWG even after the DMS preconcentration phase is over. Hence, in the IR(300)-GC-DMS setup, the experimental parameters in the IR were set to more advantageous values, thereby enhancing the IR signals. In the GC-DMS-IR(60) and the IR(60)-GC-DMS setup, all experimental parameters apart from the direction of the sample flow were the same enabling a direct comparison of the two measurement configurations in terms of their analytical performance.

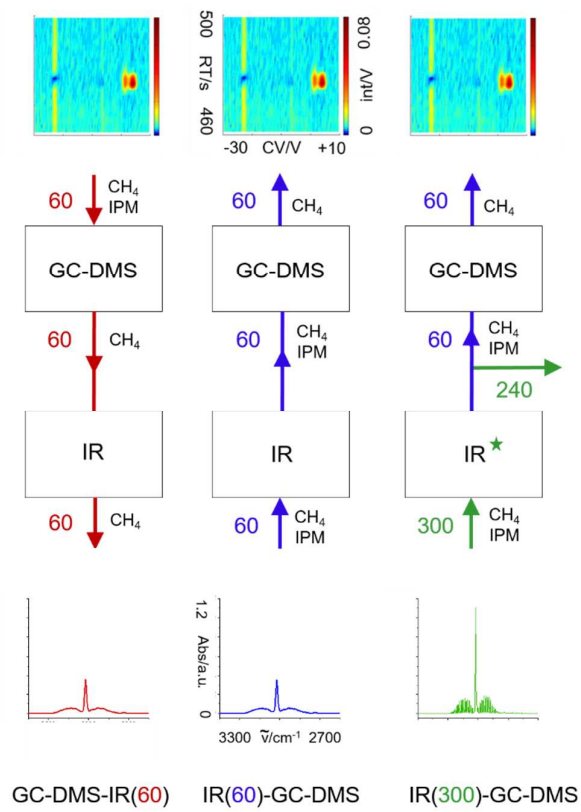

Fig. 2 Hybrid GC-DMS and iHWG-FTIR setups and respective model DMS and IR spectra. For clarity, „iHWG-FTIR" was simplified to „IR". Numbers along the flow path are listed as mL/min. In the IR(300)-GC-DMS setup, a different sample flow in the IR (300 mL/min instead of 60 mL/min) as well as different IR settings (resolution, number of averaged IR scans; symbolized by green star) were applied in order to maximize the IR signal. A detailed view of the interior of the IR and GC-DMS setups can be found in the supporting information

Concentration-dependent studies

With all three hybrid setups, concentration dependent measurement series were done. For each measurement series, a stock gas mixture of 5 ppm IPM in CH_4 was diluted to eight concentrations between 0 and 8.3 % for CH_4, and between 0 and 417 ppb for IPM using compressed air.

Accordingly, different MFCs were used in the IR(300)-GC-DMS setup versus the IR(60)-GC-DMS and GC-DMS-IR(60) setup due to the demanded flow rates. MFC performance was checked via a digital flow meter (Restek, cat.# 22656) prior to each

measurement series, and the total flow rate at the outlet of the gas mixing system was regularly checked during the experiment. Throughout, all data points were recorded five times in a random sample order that was different for the five repetitions of the measurement series. An air blank was recorded before each sample measurement. Furthermore, after each blank and after each sample measurement, a GC-DMS internal cleaning process was executed. During the GC-DMS blank measurements, the IR background spectrum was recorded for the next sample. During the cleaning process, all tubing was purged with air or the gas mixture of the subsequent sample for at least 4 min. After connecting the sample flow to the inlet valve of the GC-DMS, the GC-DMS measurement was started. 13 s later, the IR measurement was started. After the GC-DMS preconcentration phase, the sample flow was disconnected from the GC-DMS inlet.

iHWG-FTIR data processing

The evaluation of the IR data was done in Origin Pro 2017. Since the median of each data set determined to suitable represent the baseline, each IR spectrum was shifted by the median for baseline correction. The baseline-corrected IR peak of CH_4 at 3016 cm^{-1} was integrated across a spectral range from 3250 to 2600 cm^{-1}, in order to include $^{13}CH_4$ satellite peaks. For the IR measurement series, five replicates per concentration were averaged and the averaged IR peak area was plotted against the CH_4concentration, The data were fitted with a Box-Lucas function (y = a·(1-exp(-bx))). The noise was calculated as the standard deviation of the absorbance between 2600 to 3250 cm^{-1} at 0 % CH_4, and the SNR as the absorbance at 3016 cm^{-1} divided by the noise. The LOD and LOQ were calculated based on the IUPAC Compendium of Analytical Nomenclature.[35] Hence, the sum of the mean peak area at 0 % methane and $3.29 \cdot \sigma_B$ ($10 \cdot \sigma_B$ for LOQ; with σ_B being the standard deviation of the signal at 0 % CH_4, i.e. the blank) was inserted into the inverse of the Box-Lucas fit function.

GC-DMS data processing

The evaluation of the GC-DMS data was done in AnalyzeIMS (version 1.28).[36] For baseline correction, the AnalyzeIMS baseline tool based on asymmetric least square smoothing was used with the parameters λ=2 and p=0.01. For quantification of IPM, the volume of the monomer and the dimer peak were approximated by adding up the intensity values between 467 and 499 s RT and between -1.86 and +7.81 V CV. The evaluation window was selected large compared to the peak size (see Figure 4) for keeping the integration window constant for all spectra despite slight shifts of the IPM double peak along the CV and the RT axis for different spectra, and despite occasional tailing of the peak at higher concentrations. The DMS peak volume was averaged for five repetitions, the averaged DMS peak volume was plotted against the IPM concentration (see Figure 6), and a linear fit (y = A+B·x) was applied. The noise was calculated as the standard deviation of the DMS signal intensities between -1.86 and +7.81 V CV and between 467 and 499 s RT at an IPM concentration of 0 ppb. The SNR was calculated as the maximum signal intensity present within the integration limits divided by the noise. The LOD and LOQ were calculated as described for the IR data; it was assumed that the intercept of the linear fitting function was an adequate estimate for the mean peak volume of the blank.[37]

Results and Discussion

iHWG-FTIR spectra

In the recorded wavenumber regime, the absorption of CH_4 gave rise to peaks at 1304 cm^{-1} (ν_4, asymmetric bending vibration), and at 3016 cm^{-1} (ν_3, asymmetric stretching vibration).[38] The latter band was selected for quantification of CH_4 due to its higher intensity. Unlike for the GC-DMS-IR(60) and IR(60)-GC-DMS measurements, the rotational fine structure of the IR band was evident in the IR(300)-GC-DMS measurement due to the higher spectral resolution of 2 cm^{-1} (see Figure 3). Theoretically, IPM also absorbs IR light between 4000 and 400 cm^{-1};[39,40] however, due to the relatively low concentration of IPM, its IR signal was not discernible.

In the IR(300)-GC-DMS setup, the gas flow rate, the number of averaged scans, and the spectral resolution were increased compared to the other two setups.

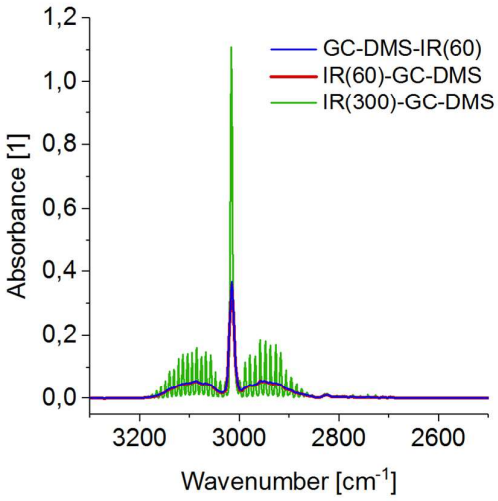

Fig. 3 IR peak at 3016 $cm^{-1}$and 4.3 % CH_4. The peak recorded with IR(300)-GC-DMS setup (green) shows rotational fine structure and higher signal intensities due to the higher resolution of 2 cm^{-1}. The peaks recorded with the IR(60)-GC-DMS and GC-DMS-IR(60) setup overlap each other and therefore cannot be clearly distinguished from one another here.

An overview on two exemplary absorbance values, the noise level, and the SNR obtained for all three setups is given in Table 1. It is evident that the results for the GC-DMS-IR(60) and the IR(60)-GC-DMS setup are in the same order of magnitude. That means, if the experimental parameters are kept constant, it is irrelevant for the IR signal, noise level, and SNR if the sample was analyzed first by the iHWG-FTIR or the GC-DMS.

Table 1 indicates that the IR(300)-GC-DMS setup results in an increased IR signal. This is due to the increased resolution.[41]

Furthermore, it is expected that a higher flow rate leads to a slightly higher analyte concentration in the iHWG resulting from the pressure difference between inlet and outlet of the iHWG, thus increasing the IR signal slightly further. As displayed in Table 1, the noise level is increased in the IR(300)-GC-DMS setup. While the increased number of averaged scans should have led to a lower noise level,[42] it is known that at higher spectral resolution, the noise level is elevated.[43] Therefore, the *noise increasing* impact of the increased resolution in the IR(300)-GC-DMS setup obviously outweighed the *noise decreasing* impact of the increased number of averaged scans (assuming that the flow rate did not have a significant influence on the noise level). Contradictory to Jaakkola *et al.*,[43] the SNR for the IR(300)-GC-DMS setup was increased vs. the other two setups (Table 1). It was expected that at increased resolution, the signal intensity and the noise increase in a way that the SNR

Table 1. Overview on experimental parameters for iHWG-FTIR and GC-DMS data.[a]

Setup	GC-DMS-IR(60)	IR(60)-GC-DMS	IR(300)-GC-DMS
IR resolution [cm^{-1}]	8	8	2
# averaged IR scans	10	10	20
IR flow rate [mL/min]	60	60	300
IR absorbance at 4.3% CH_4 [a.u.][b,c]	0.369 ± 0.0008	0.361 ± 0.006	1.104 ± 0.005
IR absorbance at 8.3% CH_4 [a.u.][b,c]	0.490 ± 0.002	0.489 ± 0.009	1.461 ± 0.009
IR peak area at 4.3% CH_4 [a.u.][c]	15.57 ± 0.06	15.13 ± 0.30	18.68 ± 0.11
IR peak area at 8.3% CH_4 [a.u.][c]	22.68 ± 0.09	22.58 ± 0.61	28.01 ± 0.04
IR Noise [a.u.]	1.924E-4	1.915E-4	2.823E-4
IR SNR at 4.3 % CH_4 [b,c]	1926	1896	3915
IR SNR at 8.3 % CH_4 [b,c]	2557	2565	5180
DMS peak volume 217 ppb IPM [a.u.][c]	1.92 ± 0.20	1.83 ± 0.17	4.06 ± 0.64
DMS peak volume 417 ppb IPM [a.u.][c]	3.08 ± 1.14	2.48 ± 0.54	5.36 ± 0.44
DMS I_{max} at 217 ppb IPM [a.u.][c,d]	0.060 ± 0.009	0.052 ± 0.012	0.167 ± 0.021
DMS I_{max} at 417 ppb IPM [a.u.][c,d]	0.126 ± 0.060	0.090 ± 0.031	0.230 ± 0.017
DMS Noise [a.u.]	1.19E-3	1.21E-3	1.19E-3
DMS SNR at I_{max} at 217 ppb [c]	51	43	141
DMS SNR at I_{max} at 417 ppb [c]	108	74	194

[a] Errors are absolute standard deviations (1σ).

[b] IR absorbance and SNR given at 3016 cm^{-1}.

[c] IR absorbances, IR peak areas, I_{max} values, DMS peak volumes and SNR values are given for two exemplarily chosen samples (4.3% CH4 / 217 ppb IPM and 8.3% CH4 / 417ppb IPM), just to give the reader an idea of the respective order of magnitude.

[d] I_{max}: max. DMS signal intensity within integration window.

overall decreases. But in our experiment, the SNR increased when going from 8 cm^{-1} to 2 cm^{-1} resolution, because we concurrently increased the number of averaged scans: the noise decreasing influence of the increased number of averaged scans compensated the noise increasing influence of the increased resolution to an extent that the noise was still higher, but that, overall, the SNR was increased in the IR(300)-GC-DMS setup. Consequently, the sequence iHWG-FTIR-GC-DMS should be used, if maximum flexibility of the flow and the IR parameters is required, e.g., for maximizing the signal and SNR during the detection of low-concentrated analytes.

GC-DMS spectra

In the DMS background spectrum, ideally only the so-called reactant ion peak (RIP) resulting from charged clusters built from the background gas components (N_2, O_2, H_2O) is evident. Having entered the DMS sensing zone, one or two analyte ions replace water molecules in the RIP clusters, thereby leading to

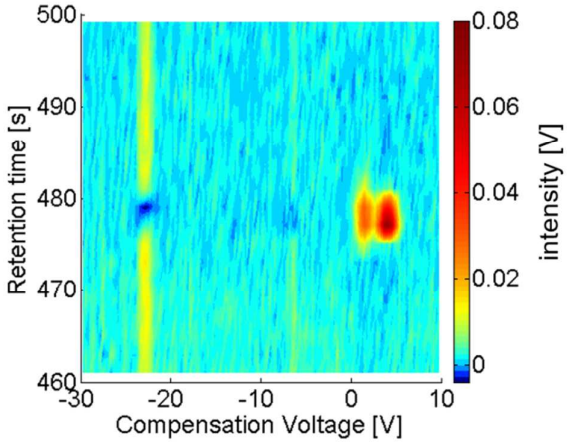

Fig. 4 DMS spectrum of 217 ppb IPM. Tentative peak assignment comprises the IPM monomer (+1.3 V CV, 479 s RT) and the IPM dimer (+3.8 V CV, 479 s RT) peak. As expected, the RIP intensity (along -23.5 V CV) is decreased while IPM is present within the DMS sensing region.

an intensity decrease of the RIP itself, and to the appearance of an analyte (monomer/dimer, respectively) peak. The positive mode GC-DMS spectrum of IPM is shown in Figure 4. As expected, the intensity of the reactant ion peak (at approx. -23.5 V CV) decreases while IPM is present in the DMS sensing zone.[44] The IPM double peak appears at a slightly shifting retention time at 479.5 ± 2.5 s comprising 30 s of preconcentration phase, and approx. 450 s of retention time at the GC column. On the basis of Nazarov *et al.*,[45] the peak at 1.3 ± 0.5 V CV was tentatively assigned to the protonated IPM monomer and the peak at 3.8 ± 0.4 V CV to the proton-bound IPM dimer. As the concentration increases, the dimer peak appears and then becomes even more intense than the monomer peak. The noise level was comparable for all three setups.

Concentration-dependent IR measurements

As evident in Figure 5, the concentration dependent IR signal curves all deviate from the straight line, which would be

expected by the Beer-Lambert law.[46] In general, according to Lothian *et al.*[46], experimental data only obey the Beer-Lambert law, i.e. show a linear trend, (a) if the incident radiation is perfectly monochromatic, (b) if no scattering occurs (optically homogeneous sample), (c) if the light beam is strictly parallel and (d) if the sample is sufficiently diluted. If the sample contains relatively high analyte concentrations, as in our case, condition (d) is not met anymore which can lead to nonlinearities of the signal. A possible pictorial explanation for the flattening of the concentration dependent IR signal curve is that the incident radiation is absorbed by sample layer after sample layer. At high concentrations, a significant portion of the light is absorbed in one sample layer, leading to a reduced light intensity in the next layer. Eventually, all the incident light intensity has been absorbed without the end of the absorption path length being reached. Therefore, a further increase of the concentration will not lead to an increase of the IR signal to the extent expected by the Beer-Lambert law, therefore leading to a flattened signal curve compared to the linear Beer

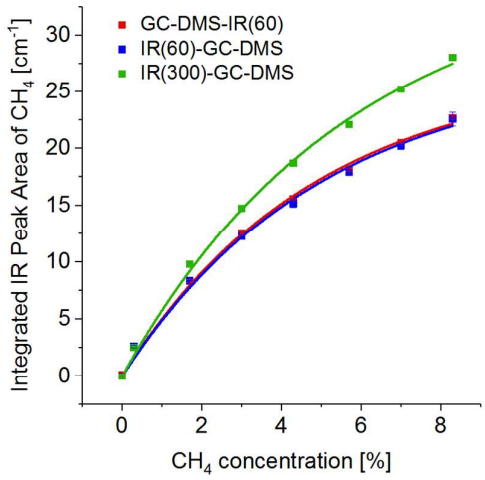

Fig. 5 Results of the concentration dependent iHWG-FTIR measurements are shown: averaged peak areas fitted with a Box-Lucas function (all R^2 > 0.99). 1σ error bars are plotted, yet hardly visible due to their small size.

Lambert shape. Also, the incident light beam can never be perfectly monochromatic (condition (a)). Furthermore, the rather moderate spectral resolution may lead to non-linearities, as well.[43] From an analytical point of view, quantification of thus obtained data is readily enabled via a non-linear curve fit. Like in Fig. 3, it can be seen in Fig. 5 that the signal intensities recorded with the IR(300)-GC-DMS setup are systematically higher than for the other two setups. The reasons – higher resolution and higher flow rate – were discussed in the section **iHWG-FTIR spectra**.

The applied Box-Lucas function (y=a·(1-exp(-bx))) resulted in R^2 values > 0.99 for all three setups. The error bars were plotted based on a single standard deviation of the five replicates (as done for the DMS data), and are barely evident due to their small size. The sensitivity of the method encoded in the slope of the IR signal curves[35] is concentration dependent, and higher for the IR(300)-GC-DMS setup versus the other two setups.

The concentration at the LOD unexpectedly was four times higher for the GC-DMS-IR(60) setup than for the other two (Table 2). Also, given the highest SNR, the IR(300)-GC-DMS setup would have been expected to result in a concentration at

Table 2. IR fit parameters, R^2 values, LOD, and LOQ

Setup	GC-DMS-IR(60)	IR(60)-GC-DMS	IR(300)-GC-DMS
Fit[a] parameter a [1]	27.225	27.312	36.035
Fit[a] parameter b [$\%^{-1}$]	0.203	0.196	0.174
R^2 >	0.995	0.994	0.997
LOD[b] [%]	0.107	0.029	0.026
LOQ[b] [%]	0.287	0.074	0.083

[a] A Box-Lucas fit (y=a·(1-exp(-bx))) was applied.

[b] The signal at the LOD and LOQ were calculated as $\mu_B+3.29\cdot\sigma_B$ and $\mu_B+10\cdot\sigma_B$, respectively, with μ_B and σ_B being the mean peak area and standard deviation of five blank measurements. The concentrations at the LOD and LOQ were calculated by inserting the signal at the LOD and LOQ into the inverse of the Box-Lucas fitting function.

the LOD/LOQ that is significantly lower than for the other two setups. However, according to the IUPAC, the approximation for

LOD and LOQ concentrations are only reliable if the data are normally distributed, have constant and known variance, if the probabilities for type I (false positive) and type II (false negative) errors are both set to 0.05, and if the uncertainty of the fitting function and the uncertainty of the blank can be neglected.[35] Since the uncertainty of the blank is too high to be negligible in the present case, the calculated mean peak area is only an estimate of its true value; likewise, the concentrations at the LOD and LOQ derived from these data are also estimates.

Concentration-dependent GC-DMS measurements

The DMS signals of the GC-DMS-IR(60) and the IR(60)-GC-DMS setup are comparable, whereas surprisingly, the DMS signals

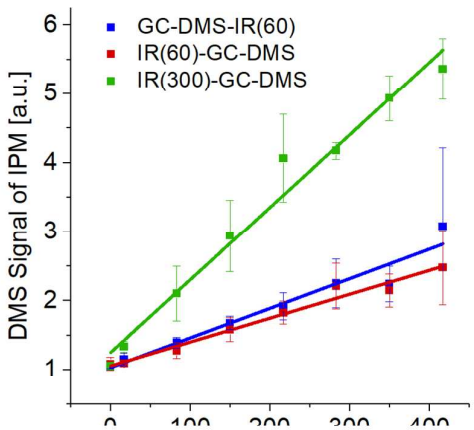

Figure 6. Results of the concentration dependent GC-DMS measurements are shown: averaged DMS peak volumes linearly fitted (all R2 > 0.94). 1σ error bars are displayed.

of the IR(300)-GC-DMS setup are higher even though the GC-DMS parameters were unchanged for all three setups. Hence, the total amount of IPM preconcentrated on the DMS preconcentration trap in the IR(300)-GC-DMS setup was apparently higher vs. the other two setups. With 300 mL/min theoretically available at the GC-DMS inlet, a larger amount of IPM may have initially reached the preconcentration trap until the DMS sampling pump adjusted to the usual 60 mL/min sampling flow (initial "overshoot" of the DMS sampling pump). Thus, more IPM appears to be preconcentrated in the IR(300)-GC-DMS setup. In the other two arrangements, only 60 mL/min was consistently available to the DMS sampling pump, and thus, even with an initial overshoot of the sampling pump, only these 60 mL/min, i.e. a lower amount of IPM than in the IR(300)-GC-DMS setup, was preconcentrated. This demonstrates that preconcentration may benefit from higher sampling rates; however, this variable is not adjustable for this particular GC-DMS unit, which relies on a simple pump to generate the flow.

Table 3. DMS fit parameters, R^2 values, LOD, and LOQ

Setup	GC-DMS-IR(60)	IR(60)-GC-DMS	IR(300)-GC-DMS
Fit[a] parameter A	1.036	1.059	1.252
Fit[a] parameter B	0.0043	0.0035	0.0105
R^2 linear fit >	0.942	0.969	0.973
LOD[b] [ppb]	32	92	14
LOQ[b] [ppb]	97	278	42

[a] A linear fit ($y = A+B\cdot x$) was applied.

[b] The signals at the LOD and LOQ were calculated as $3.29\cdot\sigma_B+\mu_B$ and $10\cdot\sigma_B+\mu_B$, respectively, with μ_B and σ_B being the mean peak volume and standard deviation of five blank measurements. The concentrations at the LOD and LOQ were calculated by inserting the signal at the LOD and LOQ into the inverse of the linear fitting function assuming that the intercept A was an adequate estimate for μ_B.

Applying a linear fit to the data leads to $R^2 > 0.94$ for all three setups. The concentrations at the LOD/LOQ were different, yet, on the same order of magnitude (low ppb range). The slope of the fit function reveals that the sensitivity of the DMS measurement in the IR(300)-GC-DMS setup was higher versus the other two setups.

Several factors may have influenced the variance for each calibration point (Figure 6). Thiols are highly reactive, rendering them difficult to detect in DMS.[47] Another contribution is the varying humidity levels within the GC-DMS, as reflected in the intensity fluctuations of the RIP.[44,48] According to Kuklya *et al.*,[48] the RIP intensity steeply increases in dependence on humidity up to approx. 100 ppm of water prior to decreasing again, since clusters of varying stability containing a different number of water molecules are formed at varying humidity levels. In data herein, the RIP intensity decreased during an entire day of measurements. Assuming that the humidity levels present in the system did not exceed 100 ppm, the GC-DMS recirculation loop was equilibrated with ambient air over night. Therefore, an equilibrated humidity level was present at the beginning of each measurement day. During the day, this humidity level was gradually decreased by adsorption of water at the silica gel within the preconcentration trap, and the humidity content in the gas samples was insufficient to compensate for this reduction. Therefore, in the future, humidity levels could be included in multivariate data evaluation strategies for addressing this issue.

Limitations of the developed hybrid iHWG-FTIR-GC-DMS method

Since the development of this hybrid technique is still in its infancy, several limitations should be overcome during future evolvements.

The GC-DMS measurement for each sample requires a comparatively long measurement time (approx. 17 min) given the GC parameters used in these experiments. This limitation could be overcome by optimizing the GC separation, which can greatly reduce the cycle time down to just a few minutes. Furthermore, time-consuming blank air measurements and internal GC-DMS cleaning processes could be avoided by a dual preconcentration trap assembly (i.e., one enriching while one is regenerating). Furthermore, an optimized sorbent material may be used optimizing the preconcentration routine, and stabilizing the humidity levels.

The iHWG-FTIR setup may benefit from an iHWG providing an extended optical path length adapted to the molar absorptivity of the molecules of interest. In addition, brighter IR light sources such as tunable quantum cascade lasers (tQCLs) and more sensitive detectors (e.g., thermoelectrically cooled mercury-cadmium-telluride semiconductor devices) would give rise to improved SNRs. Last but not least, a more constant gas flow rate throughout the entire system will benefit the robustness and reproducibility of the measurements, and minimize the associated error bars.

Conclusions

To the best of our knowledge, this study presents the first hyphenation of iHWG-FTIR and GC-DMS into an integrated analytical device. In contrast to previous studies, the developed tool is compact and robust. While other powerful techniques, such as GC-MS covering a wide range of analytes or analyte concentrations are rather expensive, the costs for the hybrid IR-DMS setup is rather moderate, especially given its analytical potential.

The presented technique takes advantage of orthogonal information provided by both analytical methods. The complementarity of addressable concentration ranges and molecular species was demonstrated using IPM and CH_4 as exemplary model analytes. Several concentration dependent measurement series in three different hybrid setups address the achievable signal intensities, SNRs, LODs, and LOQs, and illustrate strategies towards optimizing such hyphenated tools.

Future studies aim at demonstrating combined measurements in more complex vapor phase mixtures taking maximum advantage of the capabilities provided by the orthogonal combination of GC-DMS and iHWG-FTIR. A potential application scenario is the simultaneous multi-component

detection and quantification of volatile exhaled breath components.

Journal Name

ARTICLE

Conflicts of interest

There are no conflicts to declare.

Acknowledgements

This work was supported by the German Academic Exchange Service (DAAD), the Research training group PULMOSENS at Ulm University (GRK 2203) funded by the Deutsche Forschungsgemeinschaft, as well as by the German National Academic Foundation (Studienstiftung des Deutschen Volkes). Partial support was provided by: NIH award U01 EB0220003-01; NIH National Centre for Advancing Translational Sciences through award UL1 TR000002; NIH award UG3-OD023365; NIH award 1P30ES023513-01A1; NSF award 1255915; and The Northeast Gas Association. Student support was partially provided by the US Department of Veterans Affairs, Post-9/11 GI-Bill (DJP), and the National Science Foundation award 1343479 Veteran's Research Supplement (DJP). The contents of this manuscript are solely the responsibility of the author and do not necessarily represent the official views of the funding agencies. The authors would like to thank A. Wilk at IABC, Ulm Univ. for discussions on the IR data evaluation.

Abbreviations

α statistical level of Student t test, BaF_2 barium fluoride, °C degree Celsius, CH_4 methane, CV compensation voltage, DMS differential ion mobility spectrometry, DRIFT diffuse reflectance infrared Fourier transform (spectroscopy), DTGS deuterated triglycine sulfate, FAIMS high-field asymmetric waveform ion mobility spectrometry, FTIR Fourier transform infrared spectroscopy, GC gas chromatography, iHWG substrate-integrated hollow waveguide, IM ion mobility, IMS ion mobility spectrometry, IPM isopropylmercaptan, IR infrared, IRMPD Infrared Multiphoton Dissociation, λ baseline-correction parameter from AnalyzeIMS, LOD detection limit, LOQ quantification limit, μ_B mean signal of blank, MFC mass flow controller, mL/min milliliter per minute, m/z mass-to-charge ratio, OAPM off-axis parabolic mirror, p baseline-correction parameter from AnalyzeIMS, ppb parts-per-billion, ppm parts-per-million, ppt parts-per-trillioin, PTFE polytetrafluoroethylene, RF radiofrequency, RFL reflective focal length, σ_B standard deviation of blank signal, SNR signal-to-noise ratio, VOC volatile organic compound.

Notes and references

‡ Supporting Information for Publication comprises details on the iHWG-FTIR and GC-DMS setup, further results (SNR, noise etc.).

1 A. Wilk, F. Seichter, S. S. Kim, E. Tütüncü, B. Mizaikoff, J. A. Vogt, U. Wachter and P. Radermacher, *Anal. Bioanal. Chem.*, 2012, **402**, 397–404.

2 C. Charlton, A. Inberg, N. Croitoru and B. Mizaikoff, *Proc SPIE, Opt. Fibers Sensors Med. Appl. III*, 2003, **4957**, 116–123.

3 A. Wilk, J. Chance Carter, M. Chrisp, A. M. Manuel, P. Mirkarimi, J. B. Alameda and B. Mizaikoff, *Anal. Chem.*, 2013, **85**, 11205–11210.

4 J. F. Da Silveira Petruci, A. A. Cardoso, A. Wilk, V. Kokoric and B. Mizaikoff, *Anal. Chem.*, 2015, **87**, 9580–9583.

5 P. R. Fortes, J. F. Da Silveira Petruci, A. Wilk, A. A. Cardoso, I. M. Raimundo and B. Mizaikoff, *J. Opt. (United Kingdom)*, , DOI:10.1088/2040-8978/16/9/094006.

6 J. Flávio Da Silveira Petruci, P. R. Fortes, V. Kokoric, A. Wilk, I. M. Raimundo, A. A. Cardoso and B. Mizaikoff, *Analyst*, 2014, **139**, 198–203.

7 V. Kokoric, A. Wilk and B. Mizaikoff, *Anal. Methods*, 2015, **7**, 3664–3667.

8 E. Tütüncü, M. Nägele, P. Fuchs, M. Fischer and B. Mizaikoff, *ACS Sensors*, 2016, **1**, 847–851.

9 J. F. Da Silveira Petruci, A. Wilk, A. A. Cardoso and B. Mizaikoff, *Anal. Chem.*, 2015, **87**, 9605–9611.

10 B. M. Kolakowski and Z. Mester, *Analyst*, 2007, **132**, 842–864.

11 A. A. Shvartsburg, *Differential Ion Mobility Spectrometry: Nonlinear Ion Transport and Fundamentals of FAIMS*, CRC Press, Boca Raton, 2009.

12 J. Luong, E. Nazarov, R. Gras, R. A. Shellie and H. J. Cortes, *Int. J. Ion Mobil. Spectrom.*, 2012, **15**, 179–187.

13 G. A. Eiceman, E. V. Krylov, N. S. Krylova, E. G. Nazarov and R. A. Miller, *Anal. Chem.*, 2004, **76**, 4937–4944.

14 M. D. Krebs, A. M. Zapata, E. G. Nazarov, R. A. Miller, I. S. Costa, A. L. Sonenshein and C. E. Davis, *IEEE Sens. J.*, 2005, **5**, 696–703.

15 M. M. McCartney, S. L. Spitulski, A. Pasamontes, D. J. Peirano, M. J. Schirle, R. Cumeras, J. D. Simmons, J. L. Ware, J. F. Brown, A. J. Y. Poh, S. C. Dike, E. K. Foster, K. E. Godfrey and C. E. Davis, *Talanta*, 2016, **146**, 148–154.

16 A. A. Aksenov, A. Pasamontes, D. J. Peirano, W. Zhao, A. Dandekar, O. Fiehn, R. Ehsani and C. E. Davis, *Anal. Chem.*, 2014, **86**, 2481–2488.

17 M. Shnayderman, B. Mansfield, P. Yip, H. A. Clark, M. D. Krebs, S. J. Cohen, J. E. Zeskind, E. T. Ryan, H. L. Dorkin, M. V. Callahan, T. O. Stair, J. A. Gelfand, C. J. Gill, B. Hitt and C. E. Davis, *Anal. Chem.*, 2005, **77**, 5930–5937.
18 W. Zhao, S. Sankaran, A. M. Ibáñez, A. M. Dandekar and C. E. Davis, *Anal. Chim. Acta*, 2009, **647**, 46–53.
19 M. A. Molina, W. Zhao, S. Sankaran, M. Schivo, N. J. Kenyon and C. E. Davis, *Anal. Chim. Acta*, 2008, **628**, 155–161.
20 C. L. Badger, I. George, P. T. Gri, C. F. Braban, R. A. Cox and A. J. P. D, *Atmos. Chem. Phys.*, 2006, 9581–9620.
21 J. Holm and J. T. Roberts, *J. Am. Chem. Soc.*, 2007, **129**, 2496–2503.
22 D.-H. Tsai, S. Elzey, F. W. DelRio, A. M. Keene, K. M. Tyner, J. D. Clogston, R. I. MacCuspie, S. Guha, M. R. Zachariah and V. A. Hackley, *Nanoscale*, 2012, **4**, 3208.
23 L. Criado-García, R. Garrido-Delgado, L. Arce, F. López, R. Peón and M. Valcárcel, *Microchem. J.*, 2015, **121**, 163–171.
24 J. Vieillard, M. Hubert-Roux, F. Brisset, C. Soulignac, F. Fioresi, N. Mofaddel, S. Morin-Grognet, C. Afonso and F. Le Derf, *Langmuir*, 2015, **31**, 13138–13144.
25 R. J. Gustafsson, A. Orlov, C. L. Badger, P. T. Griffiths, R. a. Cox and R. M. Lambert, *Atmos. Chem. Phys. Discuss.*, 2005, **5**, 7191–7210.
26 C. L. Moss, J. Chamot-Rooke, E. Nicol, J. Brown, I. Campuzano, K. Richardson, J. P. Williams, M. F. Bush, B. Bythell, B. Paizs and F. Turecek, *J. Phys. Chem. B*, 2012, **116**, 3445–3456.
27 T. N. Le, J. C. Poully, F. Lecomte, N. Nieuwjaer, B. Manil, C. Desfrançois, F. Chirot, J. Lemoine, P. Dugourd, G. Van Der Rest and G. Grégoire, *J. Am. Soc. Mass Spectrom.*, 2013, **24**, 1937–1949.
28 J. Seo, W. Hoffmann, S. Warnke, X. Huang, S. Gewinner, W. Schöllkopf, M. T. Bowers, G. Von Helden and K. Pagel, *Nat. Chem.*, 2017, **9**, 39–44.
29 S. F. Lim, B. L. Harris, G. N. Khairallah, E. J. Bieske, P. Maître, G. Da Silva, B. D. Adamson, M. S. Scholz, N. J. A. Coughlan, R. A. J. O'Hair, M. Rathjen, D. Stares and J. M. White, *J. Org. Chem.*, 2017, **82**, 6289–6297.
30 L. Voronina, A. Masson, M. Kamrath, F. Schubert, D. Clemmer, C. Baldauf and T. Rizzo, *J. Am. Chem. Soc.*, 2016, **138**, 9224–9233.
31 J. Villatoro, M. Zühlke, D. Riebe, J. Riedel, T. Beitz and H. G. Löhmannsröben, *Anal. Bioanal. Chem.*, 2016, **408**, 6259–6268.
32 O. Hernandez, S. Isenberg, V. Steinmetz, G. L. Glish and P. Maitre, *J. Phys. Chem. A*, 2015, **119**, 6057–6064.
33 L. Voronina and T. R. Rizzo, *Phys. Chem. Chem. Phys.*, 2015, **17**, 25828–25836.
34 B. Schindler, A. D. Depland, G. Renois-Predelus, G. Karras, B. Concina, G. Celep, J. Maurelli, V. Loriot, E. Constant, R. Bredy, C. Bordas, F. Lépine and I. Compagnon, *Int. J. Ion Mobil. Spectrom.*, 2017, **20**, 119–124.
35 A. Inczédy, *IUPAC Compendium of Analytical Nomenclature: Definitve Rules. Chapter 18.4.3.7*, 3rd edn., 1997.
36 D. J. Peirano, A. Pasamontes and C. E. Davis, *Int. J. Ion Mobil. Spectrom.*, 2016, **19**, 155–166.
37 J. N. M. J.C. Miller, *Statistics and Chemometrics for Analytical Chemistry*, Pearson Education, 6th edn., 2010.
38 O. N. Ulenikov, E. S. Bekhtereva, S. Albert, S. Bauerecker, H. M. Niederer and M. Quack, *J. Chem. Phys.*, 2014, **141**, 0–33.
39 J. P. McCullough, H. L. Finke, D. W. Scott, M. E. Gross, J. F. Messerly, R. E. Pennington and G. Waddington, *J. Am. Chem. Soc.*, 1954, **76**, 4796–4802.
40 A. Pozefsky and N. D. Coggeshall, *Anal. Chem.*, 1951, **23**, 1611–1619.
41 M. Ahro and J. Kauppinen, *Appl. Spectrosc.*, 2001, **55**, 50–54.
42 J. P. Blitz and D. G. Klarup, *J. Chem. Educ.*, 2002, **79**, 1358–1360.
43 P. Jaakkola, J. D. Tate, M. Paakkunainen, J. Kauppinen and P. Saarinen, *Appl. Spectrosc.*, 1997, **51**, 1159–1168.
44 T. N. Obee, M. Piech, J. V. Mantese and S. Dardona, *Int. J. Ion Mobil. Spectrom.*, 2012, **15**, 131–139.
45 E. G. Nazarov, R. A. Miller, E. V. Krylov, J. A. Stone and G. A. Eiceman, *Int. J. Ion Mobil. Spectrom.*, 2009, **12**, 81–90.
46 G. F. Lothian, *Analyst*, 1852, **88**, 678–685.
47 K.-M. Roy, in *Ullmann's Encyclopedia of Industrial Chemistry*, Wiley VCH Verlag GmbH & Co. KGaA, Weinheim, 2012, pp. 629–655.
48 A. Kuklya, F. Uteschil, K. Kerpen, R. Marks and U. Telgheder, *Int. J. Ion Mobil. Spectrom.*, 2015, **18**, 67–75.